NASA CR-185237

ADVANCED ELECTRIC PROPULSION RESEARCH - 1989

Prepared for

LEWIS RESEARCH CENTER

NATIONAL AERONAUTICS AND SPACE ADMINISTRATION

Grant NGR-06-002-112

Annual Report

April 1990

Paul J. Wilbur
Department of Mechanical Engineering
Colorado State University
Fort Collins, Colorado 80523

NASA
National Aeronautics and Space Administration

Report Documentation Page

1. Report No.	2. Government Accession No.	3. Recipient's Catalog No.
NASA CR-185237		

4. Title and Subtitle

ADVANCED ELECTRIC PROPULSION RESEARCH - 1989

5. Report Date

April 1990

6. Performing Organization Code

7. Author(s)

Paul J. Wilbur

8. Performing Organization Report No.

10. Work Unit No.

9. Performing Organization Name and Address

Department of Mechanical Engineering
Colorado State University
Fort Collins, CO 80523

11. Contract or Grant No.

NGR-06-002-112

13. Type of Report and Period Covered

Annual
Jan. 1, 1989-Jan. 1, 1990

12. Sponsoring Agency Name and Address

National Aeronautics and Space Administration
Washington, D.C. 20546

14. Sponsoring Agency Code

15. Supplementary Notes

Grant Monitor - Vincent K. Rawlin, NASA Lewis Research Center
Cleveland, OH 44135

16. Abstract

Results of an experimental study of the characteristics of ion thruster hollow cathodes operating at high discharge currents (up to 60 A) are presented in a companion report. This work shows that ions produced near the cathode orifice can acquire sufficient energy to induce the high sputter erosion rates on cathode potential surfaces that have been observed in ion thrusters. A mechanism by which these ions could be produced is also described in this companion report. A second, brief study showing how a discharge chamber model developed previously can be applied to determine optimal values for one or more discharge chamber design parameters is presented. The experimental approach being used to study the plasma potential field and charge-exchange ion production rate downstream of the accelerator grid of an ion thruster is discussed and preliminary results are presented.

17. Key Words (Suggested by Author(s))	18. Distribution Statement
Electrostatic Ion Thruster Hollow Cathode Ion Optics	Unclassified-Unlimited

19. Security Classif. (of this report)	20. Security Classif. (of this page)	21. No of pages	22. Price*
Unclassified	Unclassified	26	

*For sale by the National Technical Information Service, Springfield, Virginia 22161

TABLE OF CONTENTS

LIST OF FIGURES

HOLLOW CATHODE OPERATION AT HIGH DISCHARGE CURRENTS

Verlin Friedly

An experimental study into the characteristics of ion thruster hollow cathodes operating at high discharge currents (up to 60 A) was conducted during the grant period. These tests showed that a hollow cathode operated at high discharge current levels can induce reduced thruster lifetimes by causing cathode insert overheating and/or erosion of surfaces located downstream of the cathode. This erosion, which has been observed in many thrusters, is known to become more severe as discharge current is increased, but the mechanism by which it could occur has not been understood. The experimental investigation conducted during the subject grant period has shown that the energies of ions produced close to the cathode orifice can be several times the anode-to-cathode potential difference generally considered available to accelerate them. These energies (of order 50 eV) are sufficient to cause the observed erosion rates. The effects of discharge current, magnetic field configuration and the cathode design and operating conditions (flowrate, orifice diameter and insert design) on the energies and current densities of these ions are examined. A qualitative description of the mechanism by which the high energy ions could be produced at modest anode-to-cathode potential differences is proposed. The effects of discharge current on cathode temperature and internal pressure are also examined experimentally and described phenomenologically. This work is described in detail in a report [1] completed during the grant period which will not be reproduced here.

A TECHNIQUE FOR OPTIMIZING DISCHARGE CHAMBER DESIGN PARAMETERS

Jeffrey Monheiser

Work was performed using the ion thruster model developed by Brophy [2] and expanded in Ref. [3] to determine the value of one of many possible design parameters that would optimize the performance of a discharge chamber for a particular mission. The design parameter selected for this particular study was the beam diameter. The specific object of the work was to determine the extent to which the screen grid of a particular thruster should be masked down to effect operation at maximum thrust-to-power on a mission for which 3000 sec was the optimal specific impulse. The discharge chamber selected for the study was an 8 cm dia. ring cusp/hollow cathode chamber on which substantial experimental data had been collected. The inner diameter of the ring magnets associated with this chamber was ~8 cm and the chamber had the physical arrangement and magnetic field configuration shown in Fig. 1.

Adjusting the beam diameter of a thruster with a prescribed discharge chamber facilitates optimization of its performance by balancing two competing effects. Those two effects are associated with neutral atom losses, which increase as the diameter is increased, and ion recombination losses on the screen grid, which decrease as the beam diameter is increased. While the optimization is carried out here in terms of beam diameter only, the technique is considered to be quite general and suitable for the selection of optimal values of one or more other discharge chamber design parameters.

In order to execute the procedure, the discharge chamber is

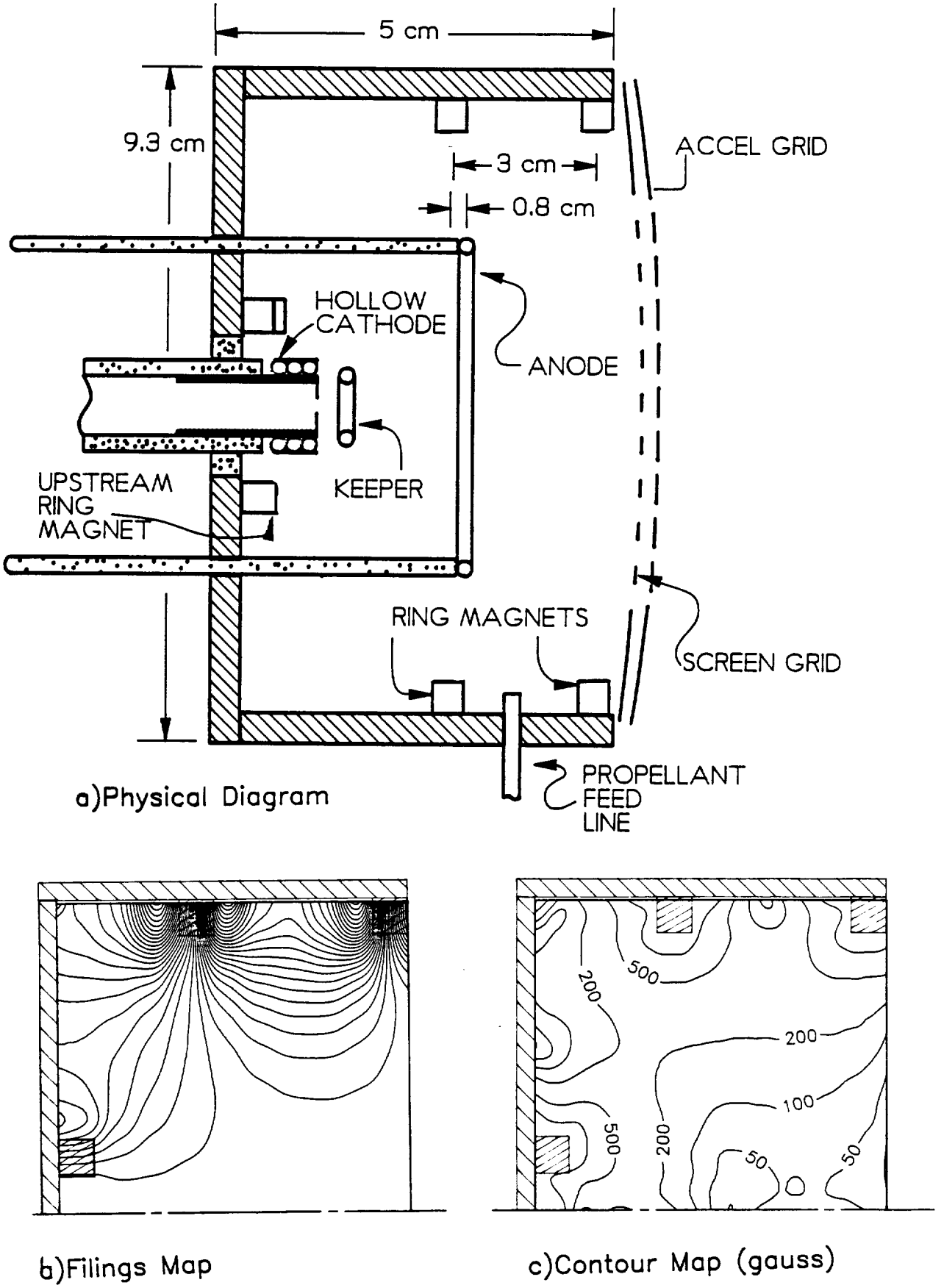

Fig. 1 8 cm Dia. Ring Cusp/Hollow Cathode Thruster

characterized as a function of the design parameter(s) of interest in terms of the performance parameters proposed by Brophy, namely, C_o, the primary electron utilization factor, ϵ_P^*, the baseline plasma ion energy cost and f_B, the fraction of the ions produced in the discharge chamber that are extracted into the beam. The relationship between these performance parameters and the beam diameter (d_B) being studied in this example could be determined from either experiments or a mathematical model relating them. For this case, the experimental results of Figs. 2 and 3 were used. They show the measured effects of beam diameter on the parameters when the discharge voltage (V_D) was being held at 40 V and xenon propellant was used. The curves of Fig. 2 depart somewhat from the ideal theoretical behavior predicted by Brophy (theoretically, ϵ_P^* should be independent of d_B and C_o should be inversely proportional to d_B^2). In spite of this and the fact that the lower plot shows some data scatter, the results will be used here as representative of the chamber.

In Fig. 3, the symbols f_S and f_W represent the fractions of ions produced that go to the screen grid and discharge chamber wall, respectively. The data in this figure show the expected complementary increase in ion losses to the screen grid and decrease in ion extraction into the beam as the beam diameter is reduced (i.e. as open area of the screen grid is reduced).

The optimization was carried out by applying the procedures and equations presented in Ref. [3]. Specifically, the propellant utilization (η_u) was selected to yield thruster operation at the maximum thrust-to-total thruster power ratio (F/P_T) as given by the expression:

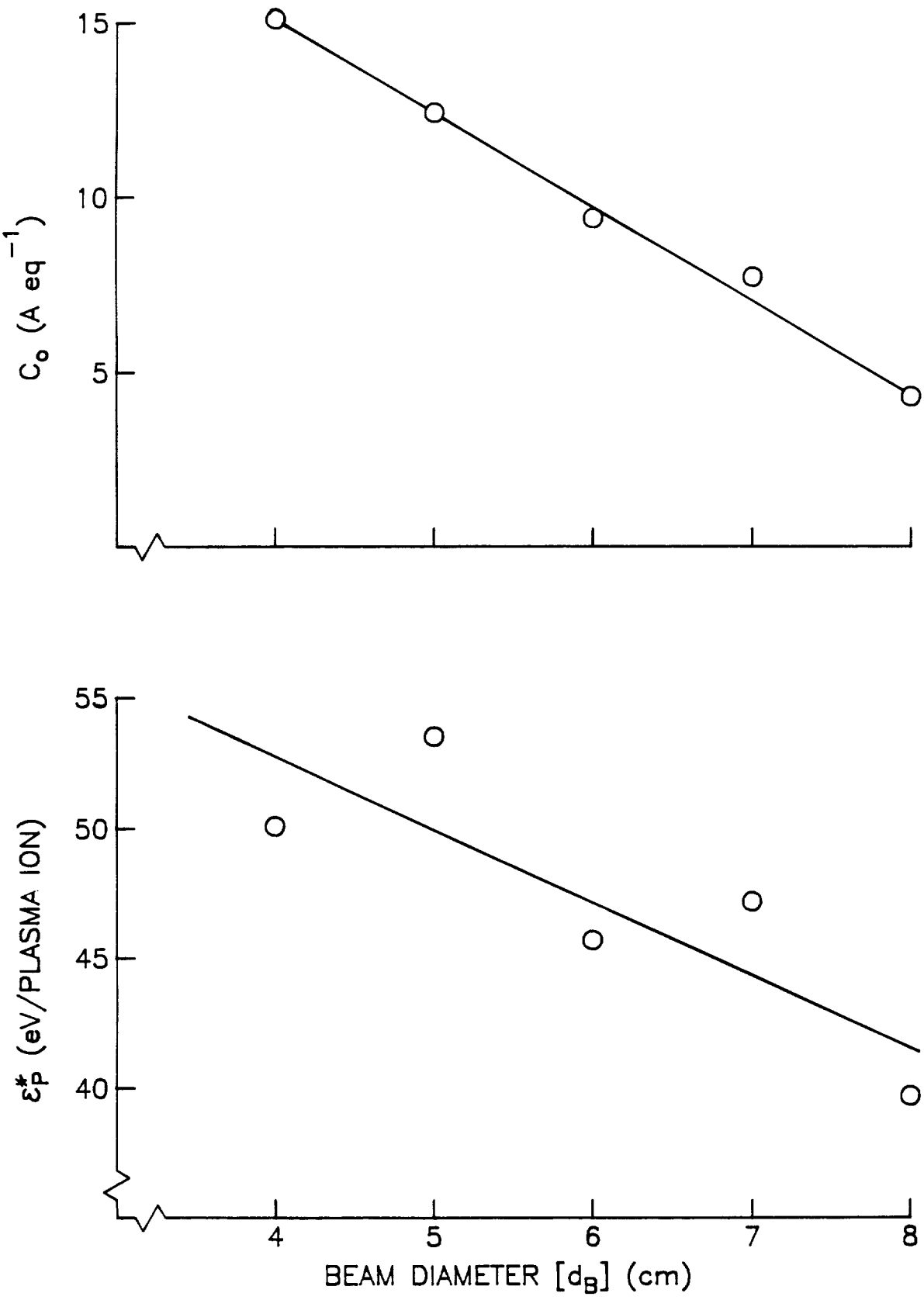

Fig. 2 Effect of Beam Diameter on Discharge Chamber Performance Parameters

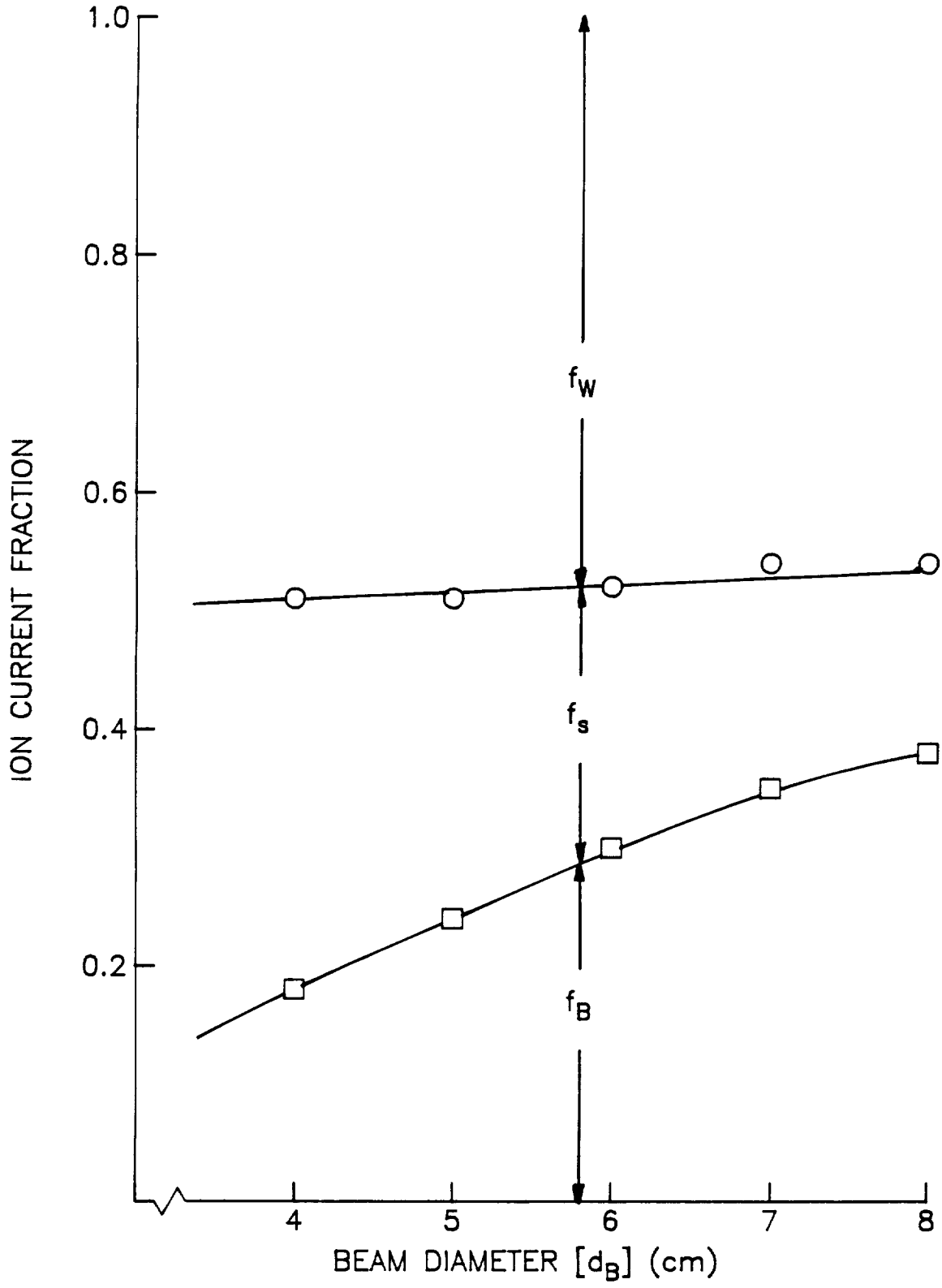

Fig. 3 Effect of Beam Diameter on Ion Current Distribution

$$\frac{F}{P_T} = \frac{I_{sp}\, g_{eo}}{\eta_u} \left[\frac{1}{\frac{1}{2}\left(\frac{I_{sp}\, g_{eo}}{\eta_u}\right)^2 + \frac{\epsilon_B e}{m_i}} \right] \qquad (1)$$

In this equation, I_{sp} is the specific impulse for the mission under consideration (3000 sec. for the present example), g_{eo} is 9.8 m/sec^2, m_i is the ion mass, and e is the electron charge. Equation 1 has been simplified here to reflect the assumption that ion beamlet divergence and doubly charged ion losses are negligible. The beam ion energy cost (ϵ_B) appearing in this equation is given by:

$$\epsilon_B = \frac{\epsilon_P^*}{f_B} \left[\left(1 - \exp\left(-\dot{m}\, C_o (1-\eta_u) \right) \right) \right]^{-1} + \frac{f_C\, V_D}{f_B} \qquad (2)$$

The fraction of the ions produced that go to cathode potential surfaces (f_C in Eq. 2) is about equal to the sum of the ion fraction going to the screen grid and chamber walls ($f_s + f_w$) which can be determined from the data of Fig. 3. The propellant flowrate ($\dot{m}$) appearing in Eq. 2 is limited to values that will assure equal atom densities at each beam area studied. It is determined using the following equation developed from related equations in Ref. [3]:

$$\dot{m} = \frac{K\, F\, d_B^2\, I_{sp}^3}{\eta_u^4} \qquad (3)$$

The coefficient K can be treated as a constant in this case where only the beam diameter (d_B) of the thruster is being changed. Values of

ion beam flatness parameter (F) required for Eq. 3 are not shown here, but they were obtained from beam current density profiles measured using a Faraday probe at each beam diameter.

The optimization procedure was carried out by varying the propellant utilization from 0.1 to 1.0 in Eqs. 1 through 3 for thrusters characterized by the performance parameters given in Figs. 2 and 3 over the beam diameter range from 5 to 8 cm. The results obtained by so doing are shown in Fig. 4. They indicate that the thruster of Fig. 1 operating at a 3000 sec. specific impulse will produce the highest thrust-to-power ratio when the beam diameter is masked down to 6 cm and the propellant utilization efficiency of about 70%. These represent increases of between 10% and 15% in both thrust-to-power ratio and propellant utilization efficiency over those associated with the largest (8 cm) diameter beam that one might ordinarily expect to yield the best thruster performance.

It is noted that the purpose of this work is to demonstrate a technique rather than to demonstrate exceptional performance. The performance of the thruster being considered in this study is rather poor by 8 cm diameter divergent or 30 cm diameter ring cusp or divergent field thruster standards even when the beam diameter is optimized. This is the case because it is a small diameter chamber and it utilizes high flux density magnets that produce strong magnetic fields that extend deep into the chamber (Fig. 1c). If the region of strong magnetic flux density were confined closer to the chamber walls, or if the discharge chamber length and diameter were greater so the depth of the penetration of the strong magnetic field was less, operation at higher thrust-to-power levels and higher propellant utilization efficiencies could be realized with a 8 cm dia. beam.

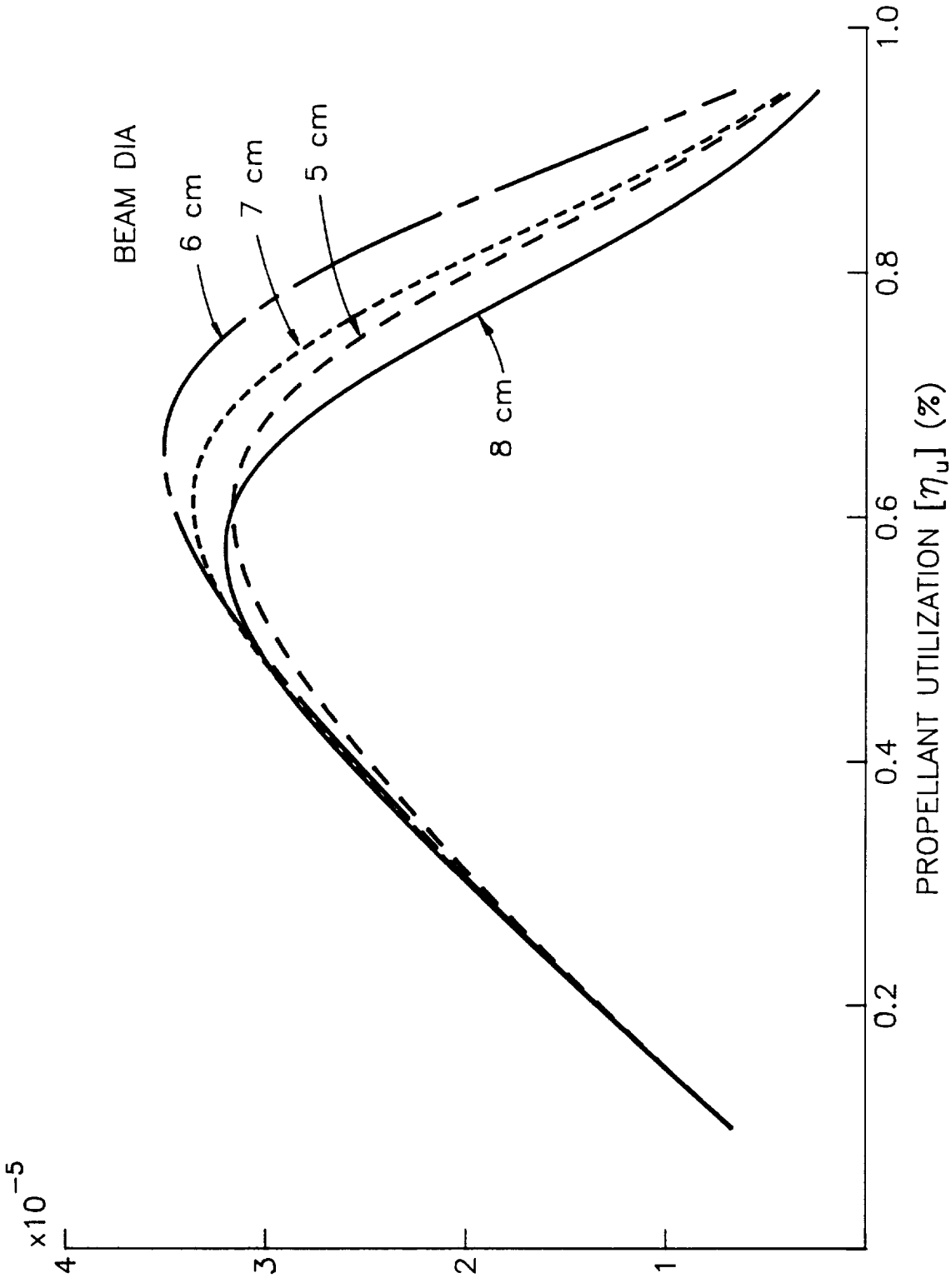

Fig. 4 Discharge Chamber Performance Optimization Curves

It is also noted that the analysis carried out here defines the maximum thrust-to-power operating point. Other objectives such as the design and operating conditions that would yield the maximum payload fraction for a particular mission could also be determined using the technique.

CHARGE-EXCHANGE ION PRODUCTION STUDY

Jeffrey Monheiser

It has been observed that accelerator grid impingement currents are significantly greater in ion thrusters that operate on xenon than they are in ones that operate on mercury. In fact, ground-based tests have suggested these currents are ~1% of the beam current when xenon is used [4] while they were only ~1/4% of the beam current with mercury [5]. This observation is of concern because it suggests that ion thruster accelerator grids that have been extensively tested on mercury may exhibit much shorter lifetimes when they are operated on xenon. It may also be, however, that this difference is due to a simple facility effect that will not be present during a space test. Specifically, it could be a reflection of the fact that xenon is more difficult to pump than mercury.

The majority of the ions that impinge on the accelerator grid of an ion thruster that is being operated properly are typically produced by the charge-exchange process in one of three regions. These regions are located 1) between the screen and accelerator grids, 2) within the apertures of the accelerator grid and 3) downstream of the accelerator grid. The fact that the charge-exchange cross sections for mercury [6] are greater than those for xenon [7,8] suggests that the impingement currents for thrusters operating on mercury should be greater than those for xenon unless the sizes of one or more of the regions of charge-exchange ion production and/or the background neutral gas or ion densities are greater when xenon is used. The volumes of the intra-grid and inter-accelerator grid regions (1 and 2)

should, however, be the same for both propellants and ion and neutral density differences are insufficient to explain the observed differences. This leads one to conclude that the size of the charge-exchange ion production region downstream of the accelerator grid may be greater when xenon rather than mercury propellant is used.

It is also possible that the size of the region from which charge-exchange ions might be drawn to the accelerator grid is influenced by a number of other factors related to the neutralizer and its operation. In order to study these effects, experiments designed to identify the effects of propellant type, flowrate and backpressure and of neutralizer position on the charge-exchange ion production environment downstream of the accelerator grid have been initiated.

The tests are being conducted on a SERT II thruster [9, 10] that has been modified by installing a 0.64 cm dia hollow cathode, separate main and cathode flow systems and a high perveance downstream-dished grid set. The grids have 1.9 mm dia. screen holes and 1.3 mm dia. accel holes on 2.2 mm centers (68% open area screen and 30% open area accel). The grid separation, which is 0.6 mm when the grids are cold, is maintained by isomica spacers that are clamped between the grids using papers clips. This grid set was made from 30 cm dia. grids that have been cut down and then masked so the beam extraction zone is 15 cm in diameter. A hollow cathode neutralizer that can be moved both radially and axially relative to the centerline and grid plane, respectively, during thruster operation has also been installed.

A schematic diagram indicating the electrical configuration of the experiment and defining the symbols used to represent the currents and voltages measured during the tests is shown in Fig. 5. In order to determine the size of the charge-exchange region from which ions

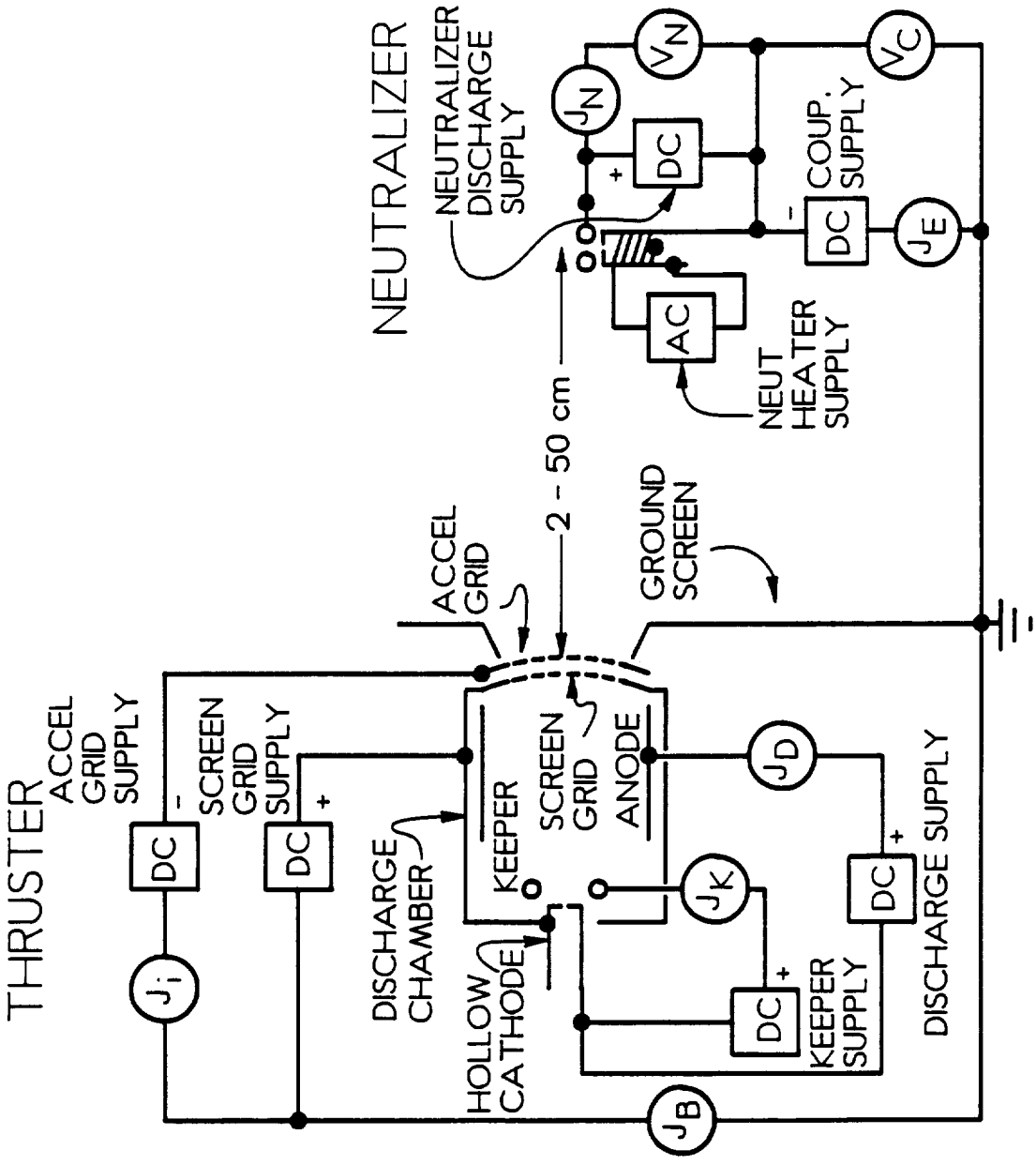

Fig. 5 Test Apparatus for Charge-Exchange Ion Production Study

are drawn to the accelerator grid, it is necessary to measure the potential field downstream of this grid. In order to measure this field, a movable emissive probe that can be swept radially through and axially parallel to the thruster centerline downstream of the grids has been installed. Applying potential contour mapping techniques to the data collected from this probe, it is hoped that the location of a ridge of maximum potential can be defined. Upstream of such a ridge one would expect the ions to be drawn into the accelerator grid, while they should flow away from it downstream of this ridge. In order to demonstrate the suitability of the apparatus, several preliminary experiments in which the thruster and neutralizer were both operated on xenon were carried out.

Figure 6 shows a typical equipotential map measured with the thruster operating at main and cathode flowrates ($\dot{m}_m$ and $\dot{m}_c$) of 270 and 145 mA eq., respectively, and a beam current (J_B) of 290 mA (i.e. at a propellant utilization efficiency (η_u) of 70%). The neutralizer was immersed in the beam at its edge and at the 5 cm axial location and emissive probe data were collected over a curved surface that did not pass close to the neutralizer location. In order to assure a neutralizer emission current that was equal to this beam current, the neutralizer bias voltage (V_c) had to be maintained at a potential 7.7 V below facility ground as indicated in the legend of Fig. 6. Other data associated with the test, positive high voltage (V_+), negative high voltage (V_-), discharge current (J_D) and discharge voltage (V_D), are also given in the legend on the figure.

The reference axial position (zero) associated with the data of Fig. 6 is the plane tangent to the dished accelerator grid at the centerline. The size of the charge exchange region, which is

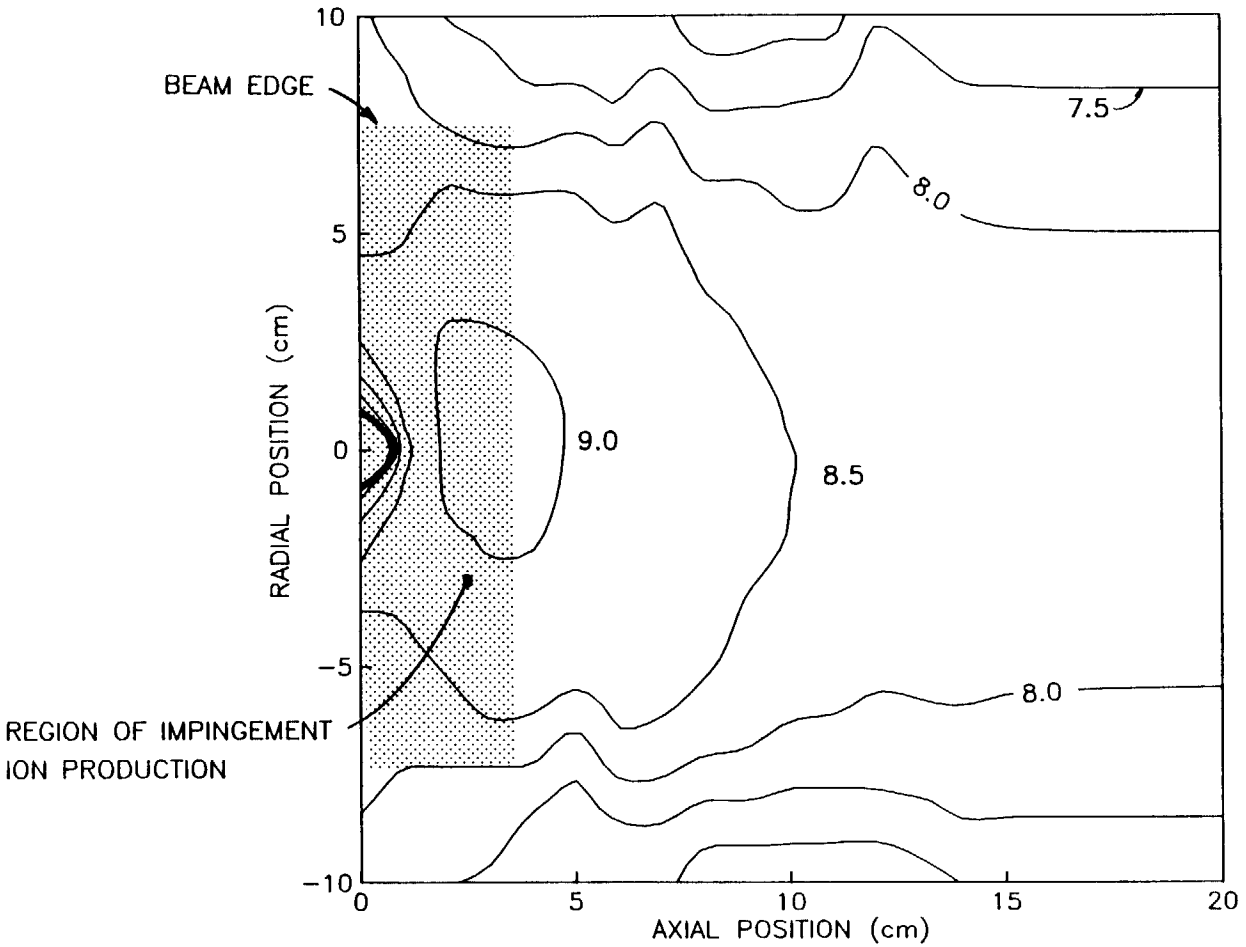

$\dot{m}_m$ = 270 mA eq.
$\dot{m}_c$ = 145 mA eq.
V_+ = 1000 V
V_- = −500 V
J_B = 290 mA
J_i = 1.8 mA
η_u = 70 %
J_D = 3.6 A
V_D = 32 V
P_o = 8×10^{-6} Torr
V_C = −7.7 V
CONTOUR POTENTIALS
IN VOLTS ABOVE GROUND

Fig. 6 Typical Potential Contour Map Downstream of an Accelerator Grid

identified by shading in the figure, extends to the anticipated potential ridge which is, therefore, about 3 cm from the grid plane at the indicated operating conditions. One would expect that charge-exchange ions produced in this region to contribute substantially to the total accelerator grid impingement current (J_i) of 1.8 mA and that those produced beyond this ridge would not.

At the present time, numerical techniques that can be applied to determine the location of the potential ridge from potential field maps and the rate of charge exchange ion production between it and the accelerator grid surface are being developed. Parameters that will be varied to determine their effect on the location of the potential ridge and the associated impingement current include: a) the propellant being used, b) the neutralizer position, c) the neutralizer axis orientation, d) the neutralizer flowrate, e) the thruster propellant flowrate and utilization efficiency and f) the ambient vacuum chamber pressure.

REFERENCES

1. Friedly, V., "Hollow Cathode Operation at High Discharge Currents," NASA CR-185238, April 1990.

2. Brophy, J. R., "Ion Thruster Performance Model," NASA CR-174810, Dec. 1984.

3. Wilbur, P. J., J. R. Beattie and J. Hyman,Jr., "An Approach to the Parametric Design of Ion Thrusters," Paper IEPC 88-080, 20th International Electric Propulsion Conference, Oct. 1988, Garmisch-Partenkirchen, West Germany.

4. Rawlin, V.K., "Internal Erosion Rates of a 10-kW Xenon Ion Thruster," AIAA Paper 88-2912, AIAA/ASME/SAE/ASEE 24th Joint Propulsion Conf., Boston, July 1988.

5. Rawlin, V.K., "Studies of Dished Accelerator Grids for 30-cm Ion Thrusters," AIAA Paper 73-1083, AIAA 10th Electric Propulsion Conference, Lake Tahoe, NV, Nov. 1973.

6. Zuccaro, D., "Measurement of Charge Exchange Cross Sections for Mercury," NASA CR-72398, Apr. 1968.

7. Smirnov, B.M. and M.I. Chibisov, "Resonance Charge Transfer in Inert Gases," Soviet Phys. Tech. Phys., V. 10, No. 1, July 1965, pp. 88-92.

8. Rapp, D. and W.E. Francis, "Charge Exchange between Gaseous Ions and Atoms," J. Chem. Phys. V. 37, No. 11, Dec. 1961, pp. 2631-2645.

9. Kerslake, W.R., Goldman, R.G. and Nieberding, W.C., "SERT II: Mission, Thruster Performance and In-Flight Thrust Measurements," J. Spacecr. Roc. V. 8, No. 3, Mar. 1971, pp. 213-224.

10. Byers, D.C. and J.F. Staggs, "SERT II Flight-Type Thruster System Performance," AIAA Paper 69-235, March 1969.

DISTRIBUTION LIST

	Copies
National Aeronautics and Space Administration Washington, DC 20546 Attn:	
RP/Mr. Earl E. VanLaningham, MS B600	1
RP/Mr. Gary Bennett, MS B600	1
RP/Mr. Marcus Watkins, MS B600	1
National Aeronautics and Space Administration Lewis Research Center 21000 Brookpark Road Cleveland, OH 44135 Attn:	
Technology Utilization Office, MS 7-3	1
Report Control Office, MS 60-1	1
Library, MS 60-3	2
Dr. M. Goldstein, Chief Scientist, MS 5-9	1
Mr. Dave Byers, MS 500-219	1
Mr. Jim Sovey, MS 500-219	1
Mr. Vincent Rawlin, MS 500-219	10
Mr. Bruce Banks, MS 302-1	1
Mr. Michael Patterson, MS 500-219	1
Mr. Tim Verhey, MS 500-219	1
National Aeronautics and Space Administration Lyndon B. Johnson Space Center Houston, TX 77058 Attn:	
Dr. James E. McCoy, Mail Code SN3	1
National Aeronautics and Space Administration Marshall Space Flight Center Huntsville, AL 35812 Attn:	
Mr. Ralph Carruth, Mail Code ES 53	1
Mr. Jason Vaughn, Mail Code ES 53	1
NASA Scientific and Technical Information Facility P.O. Box 8757 Baltimore, MD 21240 Attn:	
Accessioning Dept.	1
Dept. of the Navy Office of Naval Research University of New Mexico Bandolier Hall West Albuquerque, NM 87131 Attn:	
G. Max Irving	1

	Copies
Case Western Reserve University 10900 Euclid Avenue Cleveland, OH 44106 Attn: Dr. Eli Reshotko	1
Procurement Executive, Ministry of Defense Royal Aircraft Establishment Farnborough, Hants GU14 6TD ENGLAND Attn: Dr. D. G. Fearn	1
United Kingdom Atomic Energy Authority Culham Laboratory Abingdon, Oxfordshire OX143DB ENGLAND Attn: Dr. A. R. Martin (Rm F4/135)	1
Intelsat 3400 International Dr. N.W. Washington D.C. 20008-3098 Attn: Mr. Bernard Free, MS 33	1
Air Force Astronautics Lab Edwards AFB, CA 93523 Attn: LSVE/Mr. J. Chris Andrews LKDH/Lt. Phil Roberts, MS 24	1 1
Giessen University 1st Institute of Physics Giessen, West Germany Attn: Professor H. W. Loeb	1
Jet Propulsion Laboratory 4800 Oak Grove Laboratory Pasadena, CA 91109 Attn: Technical Library Mr. James Graf Dr. John Brophy, MS 125-224 Dr. Charles Garner, MS 125-224	1 1 1 1
TRW Inc. TRW Systems One Space Park Redondo Beach, CA 90278 Attn: Mr. Sid Zafran	1

	Copies
National Aeronautics and Space Administration Ames Research Center Moffett Field, CA 94035 Attn:	
Technical Library	1
National Aeronautics and Space Administration Langley Research Center Langley Field Station Hampton, VA 23365 Attn:	
Technical Library	1
Hughes Research Laboratories 3011 Malibu Canyon Road Malibu, CA 90265 Attn:	
Dr. Jay Hyman, MS RL 57	1
Dr. J. R. Beattie, MS RL 57	1
Dr. J. N. Matossian, MS RL 57	1
Engineering Quadrangle Princeton University Princeton, NJ 08540 Attn:	
Prof R. G. Jahn	1
Dr. Arnold Kelly	1
Boeing Aerospace Co. P. O. Box 3999 Seattle, WA 98124-2499 Attn:	
Dr. J.S. Meserole, MS 82/83	1
Lockheed Missiles and Space Co. Sunnyvale, CA 94088 Attn:	
Dr. William L. Owens, Dept. 57-24	1
Rocket Research Co. P.O. Box 97009 Redmond, WA 98073-9709 Attn:	
Mr. William W. Smith	1
Mr. Paul Lichon	1
Dr. Dave King	1
Electrotechnical Laboratory 1-1-4, Umezono, Tsukuba-Shi Ibaraki, 305 JAPAN Attn:	
Dr. Isao Kudo	1

	Copies
Sandia Laboratories P. O. Box 5800 Albuquerque, NM 87185 Attn:	
Mr. Ralph R. Peters, Mail Code 4537	1
Mr. Dean Rovang, Mail Code 1251	1
Ion Tech Inc. 2330 E. Prospect Road Fort Collins, CO 80525 Attn:	
Dr. Gerald C. Isaacson	1
Dr. Dan Siegfried	1
Mr. Larry Daniels	1
EG & G Idaho P. O. Box 1625 Idaho Falls, ID 83401 Attn:	
Dr. G. R. Longhurst, TSA-104	1
Michigan State University East Lansing, MI 48824 Attn:	
Dr. J. Asmussen	1
Dr. M.C. Hawley	1
Aerospace Engineering Department Faculty of Engineering Tokai University Kitakanome, Hiratsuka-shi, Kanagawa-ken, JAPAN 259 Attn:	
Prof. Itsuro Kimura	1
Department of Electronics Tokyo National Technical College No. 1220-2 Kunugida-cha, Hachioji 193 Tokyo, JAPAN Attn:	
Mr. Susumu Masaki	1
Tuskegee Institute School of Engineering Tuskegee Institute, AL 36088 Attn:	
Dr. Pradosh Ray	1
Mr. Lee Parker 252 Lexington Road Concord, MA 01741	1

	Copies
Physics Department Naval Postgraduate School Monterey, CA 93943-5000 Attn: Dr. Chris Olson, Mail Code 61-OS	1
Martin Marietta Aerospace P. O. Box 179 Denver, CO 80201 Attn: Dr. Kevin Rudolph, MS M0482	1
S-Cubed P. O. Box 1620 LaJolla, CA 92038 Attn: Dr. Ira Katz	1
Dept. of Aero. & Astro. Engineering 101 Transportation Bldg. 104 South Mathews Ave. Urbana, IL 61801-2997 Attn: Dr. Rodney Burton	1
Instituto de Pesquisas Espaciais - INPE Library and Documentation Division C.P. 515 Sao Jose dos Campos - SP 12200 - BRAZIL	1
Tektronix Inc. P.O. Box 500 Beaverton, OR 97077 Attn: Mr. Curtis Haynes, MS 50-324	1
Dr. Robert Vondra P.O. Box 596 Wrightwood, CA 92397	1
Electric Propulsion Laboratory, Inc. 43423 N. Division St., Suite 205 Lancaster, CA 93535 Attn: Dr. Graeme Aston	1
Department of Aeronautics University of Tokyo 7-3-1 Hongo, Bunko-ku Tokyo 113, Japan Attn: Prof. Yoshihiro Arakawa	1

	Copies
University of Tennessee Space Institute Tullahoma, TN 37388-8897 Attn: Mr. Verlin Friedly Center for Aerospace Research	1
National Aerospace Laboratory of Japan 7-44-1 Jindaijihigashi-Machi Chofu Tokyo, 182, Japan Attn: Mr. Yukio Hayakawa	1